

Layer-Number-Dependent Effects of Graphene Oxide on the Pluripotency of Mouse Embryonic Stem Cells Through the Regulation of the Interaction Between the Extracellular Matrix and Integrins

Guoxin Jing¹
Kun Li¹
Feiyue Sun¹
Jintong Niu¹
Rongrong Zhu¹
Yechang Qian²
Shilong Wang¹ 

¹Research Center for Translational Medicine at East Hospital, School of Life Science and Technology, Tongji University, Shanghai, People's Republic of China;

²Department of Respiratory Disease, Baoshan District Hospital of Integrated Traditional Chinese and Western Medicine, Shanghai, People's Republic of China

Introduction: Embryonic stem cells (ESCs) possess great application prospects in biological research and regenerative medicine, so it is important to obtain ESCs with excellent and stable cellular states during in vitro expansion. The feeder layer culture system with the addition of leukemia inhibitory factor (LIF) is currently applied in ESC cultures, but it has a series of disadvantages that could influence the culture efficiency and quality of the ESCs. With the development of nanotechnology, many studies have applied nanomaterials to optimize the stem cell culture system and regulate the fate of stem cells. In this study, we investigated the layer-number-dependent biofunction of graphene oxide (GO) on the pluripotency of ESCs from mice (mESCs).

Methods: Single-layer GO (SGO) and multi-layer GO (MGO) were characterized and their effects on the cytotoxicity and self-renewal of mESCs were detected in vitro. The differentiation potentials of mESCs were identified through the formation of embryoid bodies and teratomas. The regulatory mechanism of GO was verified by blocking the target receptors on the surface of mESCs using antibodies.

Results: Both SGO and MGO were biocompatible with mESCs, but only MGO effectively sustained their self-renewal and differentiation potential. In addition, GO influenced the cellular activities of mESCs by regulating the interactions between extracellular matrix proteins and integrins.

Conclusion: This work demonstrates the layer-number-dependent effects of GO on regulating the cell behavior of mESCs and reveals the extracellular regulatory mechanism of this process.

Keywords: mouse embryonic stem cell, graphene oxide, extracellular matrix, integrins

Introduction

Embryonic stem cells (ESCs) are derived from the inner cell mass (ICM) of the blastocyst at an early stage during embryonic development. They have the ability of infinite self-renewal and the differentiation potential to form three germ layer cells.¹ The successful establishment of ESCs has tremendous application value in biomedical research, such as research in embryonic development, establishment of disease models, the development of drugs and the treatment of diseases.² However, ESCs

Correspondence: Yechang Qian; Shilong Wang
Tel +86 2165918108; +86 2165982595
Fax +86 2136070892; +86 2165982595
Email qianyechang@163.com; wsl@tongji.edu.cn



still confront a series of challenges before they could be applied in clinic³ and one of the challenge is the cultivation of ESCs in vitro is prone to spontaneous differentiation. Therefore, it is of great significance to control the state of ESCs in vitro accurately for the clinical application of them.⁴ With the development of nanotechnology in recent years, applying nanomaterials to regulate the cell behavior of ESCs and optimize the traditional cell culture system has become an important focus of stem cell research.^{5–8}

The amplification of mESCs in vitro can be divided into a feeder layer culture system and feeder-free culture system. Feeder layer cells (feeders) are monolayer cells with an inhibitory mitotic ability obtained by certain chemical or physical treatment. Feeders can secrete extracellular matrix (ECM) proteins, adhesion factors, and a variety of cytokines, such as leukemia inhibitory factor (LIF),^{9,10} fibroblast growth factor (bFGF), bone morphogenetic protein 4 (BMP4), and others. These factors can provide an ideal extracellular growth environment for mESCs to maintain their proliferation, adhesion, and self-renewal abilities.^{11,12} LIF belongs to the IL-6 family of cytokines and can initiate cascade signaling to sustain the pluripotency of mESCs by co-binding with glycoprotein 130 (gp130) and LIF receptor (LIFR).^{13,14}

ECM components are also important candidates for regulating the proliferation, adhesion, self-renewal, and differentiation of ESCs.^{15,16} Integrins are cell surface receptors that mediate ECM adhesion and transfer the extracellular signals to the intracellular space.¹⁷ Integrins are heterodimer transmembrane proteins composed of α and β subunits.¹⁸ The extracellular domains of integrins are capable of binding to ECM ligand proteins such as laminin, fibronectin (FN), collagen, and vitronectin, while their intracellular domains are capable of binding to cytoskeleton proteins (eg, α -actinin, talin) and other regulatory proteins (eg, cadherin, cell adhesion proteins).¹⁹ The interaction between the ECM ligand and integrin receptor can activate an intracellular signaling response and induce cytoskeletal changes, thus regulating the behavior of stem cells.¹⁷ FN is an important component of ECM, which regulates a variety of cell activities by direct interaction with the integrin receptor. FN is critical during the process of vertebrate development because it mediates a variety of cell interactions and plays an important role in cell adhesion, migration, propagation, and differentiation.^{20,21} Integrin $\alpha 5\beta 1$ is a crucial FN-specific receptor involved in the regulation of the differentiation of

stem cells, such as osteogenic differentiation.²² In a previous study, exogenous FN was successfully used to stimulate the integrin signaling pathway and promote the differentiation of mESCs.²³

Graphene is a two-dimensional honeycomb lattice composed of sp^2 -hybridized carbon atoms. Graphene oxide (GO) is the oxidation product of graphene, and its surface contains various oxygen functional groups.^{24,25} GO has good biological properties, such as hydrophilicity, biocompatibility,²⁶ and easy functionalization.²⁷ Due to its unique physicochemical properties, many researchers have attempted to reveal its biofunction in stem cells.^{28,29} GO-based nanomaterials can regulate the growth and differentiation of stem cells in the form of nanoparticle suspensions, 2D substrates, and 3D scaffolds.³⁰ The biofunction of GO in stem cells is influenced by its physicochemical properties, such as solution concentration,³¹ particle size,^{32,33} shape,³⁴ oxidation degree,^{35,36} and surface modification.^{37,38} The layer thickness determined by the number of GO sheets is an important property of the material and its derivatives, as it can affect physical properties such as morphology, surface properties, electrical conductivity, and mechanical properties (bending ability and flexibility).^{39,40} There has been no relevant research on the regulation of GO sheet thickness on stem cells. In previous work, we have found that GO can sustain the self-renewal of mESCs and have revealed its intracellular regulatory mechanisms. However, how GO interacts directly with mESCs has remained a persistent question. Hence, in this study, we explored the effect of GO sheet thickness on the pluripotency of mESCs and further investigated the interaction between GOs and the ECM of cells (Scheme 1).

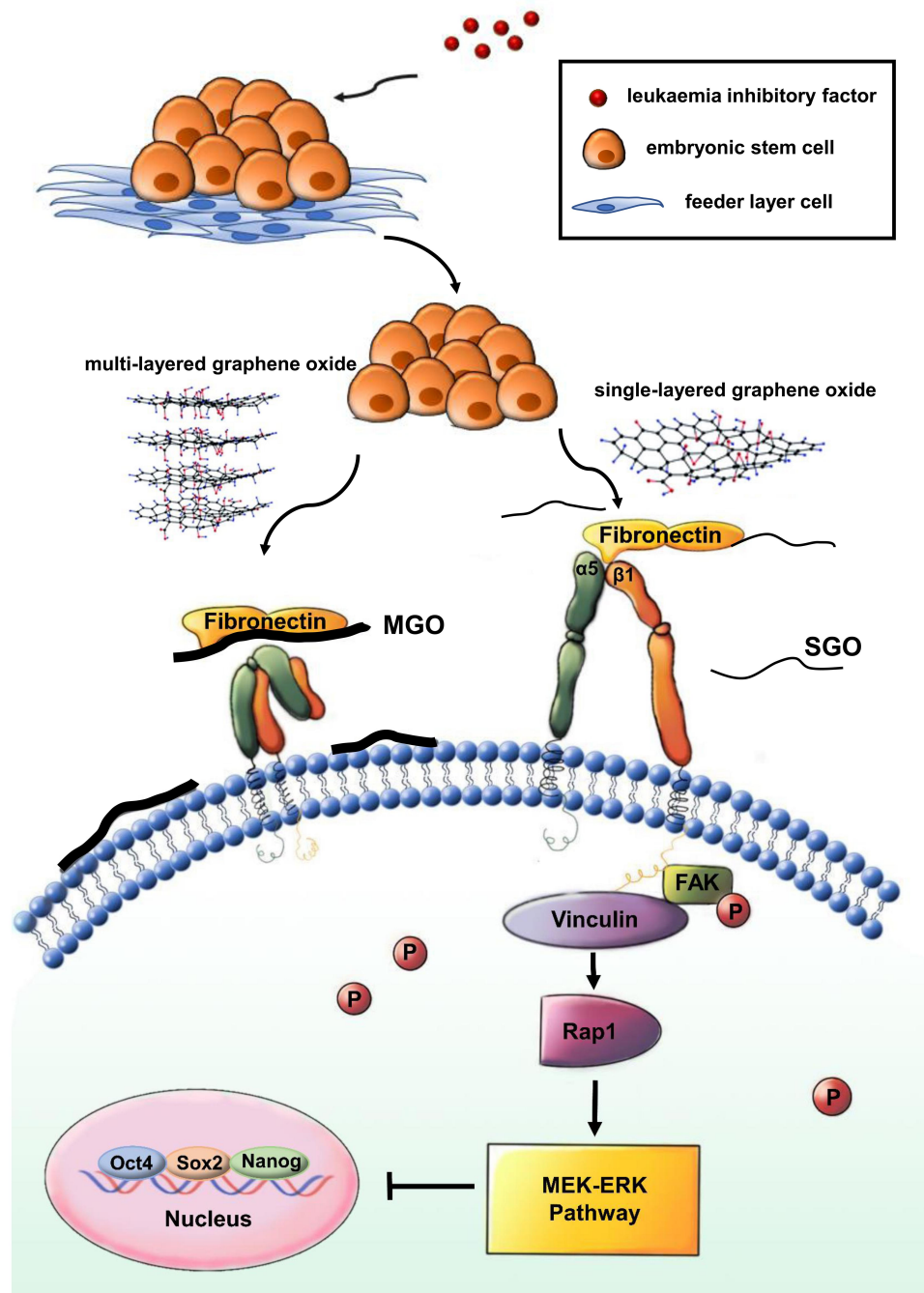
Materials and Methods

Characterization of GO

MGO was purchased from Aladdin[®] and SGO was purchased from XFNano[®]. The morphologies of the materials were observed by transmission electron microscopy (TEM) (JEM-F200, JEOL). Atomic force microscopy (AFM) (and SPM-9600, Shimadzu) was also applied to detect the thickness of the samples. X-ray photoelectron spectroscopy (XPS) (ESCALAB 250XI, Thermo Fisher) was performed to analyze the elemental content of the samples.

Mouse Embryonic Stem Cell Culture

The mESC line 46C was gifted by Dr. Xiaoqing Zhang (Tongji University, Shanghai, China), and the use of cells



Scheme 1 Schematic diagram of graphene oxide with different layer numbers regulating the cell behavior of mouse embryonic stem cells.

was approved by the Ethical Committee of Tongji University of Medicine. The mESCs were cultured on γ -irradiated feeder cells, and the culture medium contained high-glucose DMEM (Gibco) with 15% fetal bovine serum (Gibco), 1 mM L-glutamine (Gibco), 1% nonessential amino acids (Gibco), 0.1 mM β -mercaptoethanol (Gibco), and 1000 U/mL LIF (Millipore). The trypsinized mESCs were planted on 0.1% gelatin-coated culture plates

for 15 min to make feeder cells adhere to the plate. Non-adhered mESCs were collected and replanted on 0.1% gelatin-coated culture plates at a concentration of 1×10^4 cells/mL. GOs were supplemented overnight, and the culture medium was replaced every other day. The confluent cultures were trypsinized with 0.25% trypsin-EDTA usually after 4–5 days of proliferation. For long-term culturing, mESCs were passaged for 3–4 days. The cells

were trypsinized and plated (2×10^4 cells) onto fresh, gelatin-coated, 6-well plates. The medium was refreshed every day with the addition of GOs suspension.

CCK-8 for Detecting Cell Proliferation

The mESCs were trypsinized into single cells and feeder cells were removed. The mESCs were placed into gelatin-treated 96-well plates at a density of 4×10^3 cells/well. The cells were cultured for 1–2 days, and the culture medium, with SGO or MGO additions at concentrations of 8, 16, and 32 $\mu\text{g/mL}$, was replaced daily. After either 24 or 48 h of GOs treatment, 10 μL CCK-8 cell proliferation detection solution was added into each well and incubated at 37°C for 1–4 h. The absorbance of each well was detected with 450 nm excitation. The cell survival rate (%) was calculated as $\text{OD}_{450}(\text{experimental group})/\text{OD}_{450}(\text{blank control group}) \times 100\%$.

Annexin V-FITC/PI for Detecting Cell Apoptosis

The mESCs were incubated with 4, 8, 16, and 32 $\mu\text{g/mL}$ SGO or MGO for 48 h. Then the cells were collected after being trypsinized by 0.25% trypsin EDTA and then labeled with an Annexin V-FITC/PI Apoptosis Detection Kit (KeyGEN BioTECH). Apoptosis detection was performed using a FACScan flow cytometer (BD Biosciences). The results were analyzed using the Flowjo software.

Alkaline Phosphatase Staining Assay

The culture medium was aspirated off and the cells were washed with PBS two to three times. The cells were fixed with 4% paraformaldehyde (PFA) for 1–2 min and then washed with PBS and TBST twice. The bottom of the plate was covered using sufficient alkaline phosphatase reagent (Yeasen) dying solution, which was then incubated for 15–20 min at room temperature and stored in PBS. The results were recorded via microscope.

Quantitative Real-Time PCR (RT-PCR)

The total RNA was extracted through a series of purifications and ultimately stored in DEPC-water. Its concentration was quantified using Nanodrop. The Primer Script Reverse Transcriptase Kit (Takara) was used to reverse-transcribe RNA into cDNA. Then RT-PCR was performed using the TB Green Premix Ex Taq™ (Takara) reaction system on the ABI7500 Real-Time PCR System. *Gapdh* acted as an internal reference.

Western Blot Analysis

Total protein was extracted using an extraction kit (KeyGEN BioTECH), and its concentration was quantified using the BCA method. The protein samples were separated by SDS-PAGE and then transferred to PVDF membranes (Millipore). The membranes were separately incubated with rabbit anti-OCT4 (1:2000, Abcam), rabbit anti-NANOG (1:2000, Abcam), rabbit anti-SOX2 (1:2000, Abcam), mouse anti-SSEA-1 (Santa Cruz), mouse anti-ESRRB (Santa Cruz), rabbit monoclonal anti-p-FAK (phospho Y397, 1:1000, Abcam), rabbit anti-p-ERK1/2 (phospho-Thr202/Tyr204, 1:2000, Abcam), rabbit anti-RAP1 (1:2000, Abcam), rabbit anti-vinculin (1:2000, Abcam), rabbit anti-integrin $\beta 1$ (1:2000, Abcam), rabbit anti-integrin $\alpha 5$ (1:2000, Abcam), and mouse monoclonal anti- β -actin (1:2000, CMC TAG). Horseradish peroxidase-conjugated antibody to mouse IgG or rabbit antibody to goat IgG (1:2000, Cell Signaling Technology) were used as secondary antibodies. Immunoblots were visualized using the ECL reagent (Thermo Fisher) and imaging through an ImageQuant LAS 4000 mini (GE Healthcare Life Sciences).

Immunofluorescence Staining

The cells were fixed with 4% paraformaldehyde for 15–20 min at room temperature and permeabilized with 0.2% Triton X-100 for 5–10 min before incubating them with 1% goat serum (Beyotime) at room temperature for 1 h to block unspecific binding sites. Then they were incubated with primary antibodies at 4°C overnight as follows: rabbit anti-OCT4 (1:500, Abcam), rabbit anti-NANOG (1:500, Abcam), rabbit anti-SOX2 (1:500, Abcam), rabbit anti-integrin $\beta 1$ (1:2000, Abcam), rabbit anti-integrin $\alpha 5$ (1:2000, Abcam), and rabbit anti-Vinculin (1:2000, Abcam). Then the samples were incubated in secondary antibodies, either FITC-conjugated goat anti-rabbit antibody or FITC-conjugated goat anti-mouse antibody (1:100, Millipore), which were diluted in 1% goat serum. The nuclei were labeled with DAPI. The samples were observed under a fluorescence microscope (ECLIPSE Ti, Nikon) or with confocal microscopy (LSM880, Carl Zeiss) to observe their phase and fluorescence.

Embryoid Body Formation

The mESCs treated with 16 $\mu\text{g/mL}$ GOs for 3 days were collected after being trypsinized as single cells. The cells

were cultured in differential culture medium (with 15% fetal bovine serum, 1 mM L-glutamine [Gibco], and 1% nonessential amino acids in high-glucose DMEM). Embryonic, body-like spheres formed after 3 days were detected under the microscope.

Teratoma Formation

The mESCs treated with 16 $\mu\text{g/mL}$ GOs for three passages were collected and dispersed in DMEM supplemented with 50% matrigel at a concentration of 5×10^5 cells per 100 μL . Then, 5×10^5 cells were subcutaneously injected into the hind limb of NOD-SCID mice (female). The mice were sacrificed after 4 weeks, and their tumors were peeled off. All experiments were performed in compliance with the relevant laws and institutional guidelines and approved by the International Animal Care and Use Committee at the Shanghai Institute of Materia Medica, Chinese Academy of Sciences.

Cellular Uptake of Graphene Oxide

First, 5 mg EDC and 10 mg NHS were separately dissolved in 2 mL SGO and MGO. The solution was stirred for 2 h at room temperature and then centrifuged at 2×10^4 rpm for 10 min. The supernatant was removed and the deposit was dissolved in 2 mL FITC-BSA solution at a concentration of 0.1 mg/mL, stirring the mixed solution at 2×10^4 rpm for 10 min. The deposit was FITC-labeled SGO or MGO. The product was dissolved in 100 μL ddH₂O and stored at 4°C for later use. The FITC-labeled SGO or MGO were co-incubated with mESCs for 16 h. The cell membranes were labeled with Dil and the nuclei were stained with DAPI. The distribution of GO in the mESCs was monitored using a confocal microscope.

Assay of Protein Adsorption Capacity of GOs

First, 0.4 mg/mL SGO or MGO was mixed with FBS, BSA (100 $\mu\text{g/mL}$), and FN (50 $\mu\text{g/mL}$) at a volume ratio of 1:1 and incubated for 3 h at 37°C. Then the samples were centrifuged at 2×10^4 rpm at 4°C for 30 min. The deposit was washed with washing buffer (800 mM KCl and 0.01% twain 20 dissolved in 1×PBS) three times to remove unbound proteins. Proteins bound on the materials were quantified using the BCA method or detected the morphology by TEM.

Blocking Integrins

The feeder-free mESCs were cultured with the addition of rabbit anti-integrin $\alpha 5$ (with a dilution ratio of 1:500, BioCell) and mouse anti-integrin $\beta 1$ (at a concentration of 5 $\mu\text{g/mL}$, Abcam) for 3 days, then either total RNA or total protein were collected for further detection.

Statistical Analysis

The data are shown as the mean \pm SEM of more than three independent duplicates. One-way analysis of variance was used to determine statistical significance, and a Tukey post-test followed to compare all of the conditions with each other. Tests were performed using GraphPad Prism 6.

Results and Discussion

Characterization of GOs with Different Sheet Thicknesses

To investigate the effect of GO sheet thickness on mESCs, we prepared single-layer GO (SGO) and multi-layer GO (MGO). The surface morphology and size of each were observed by TEM and AFM (Figure 1A, B and C). The layers of both were stacked together, and the shape of their edges was irregular. Both materials were not uniform in size; compared to MGO, SGO was much thinner and more flexible, so it presented more obvious folds. The AFM images also showed that the sheet thickness of MGO was greater than that of SGO, being 0.7–1.2 nm (1.195 nm) in the latter, which conforms to the characteristics of a typical SGO. The thickness of MGO was about 3.19 nm.

Zeta potential distribution analysis of SGO and MGO was also supplemented in Figure S1 to exhibit the surface charge of GOs. The results exhibited that the average zeta potential of SGO and MGO are -14.6 mV and -13.3 mV respectively, which represent no significant difference.

Raman spectroscopy detection is highly sensitive to geometric structure and chemical bonding within molecules, which makes it useful for exploring the different allotropes of carbons. The Raman spectra of GOs displayed two characteristic peaks, which were separately distributed among $1300\text{--}1400$ cm^{-1} and $1560\text{--}1620$ cm^{-1} , representing the D-band and G-band, respectively. The position of the G-band was extremely sensitive to the number of GO layers; thus, we compared the thickness of samples by observing the relative position of the G-band.^{41,42} Its position was at 1583 cm^{-1} for MGO and 1590 cm^{-1} for SGO (Figure 1D). This is because, as the sheet thickness increased, the band position shifted to

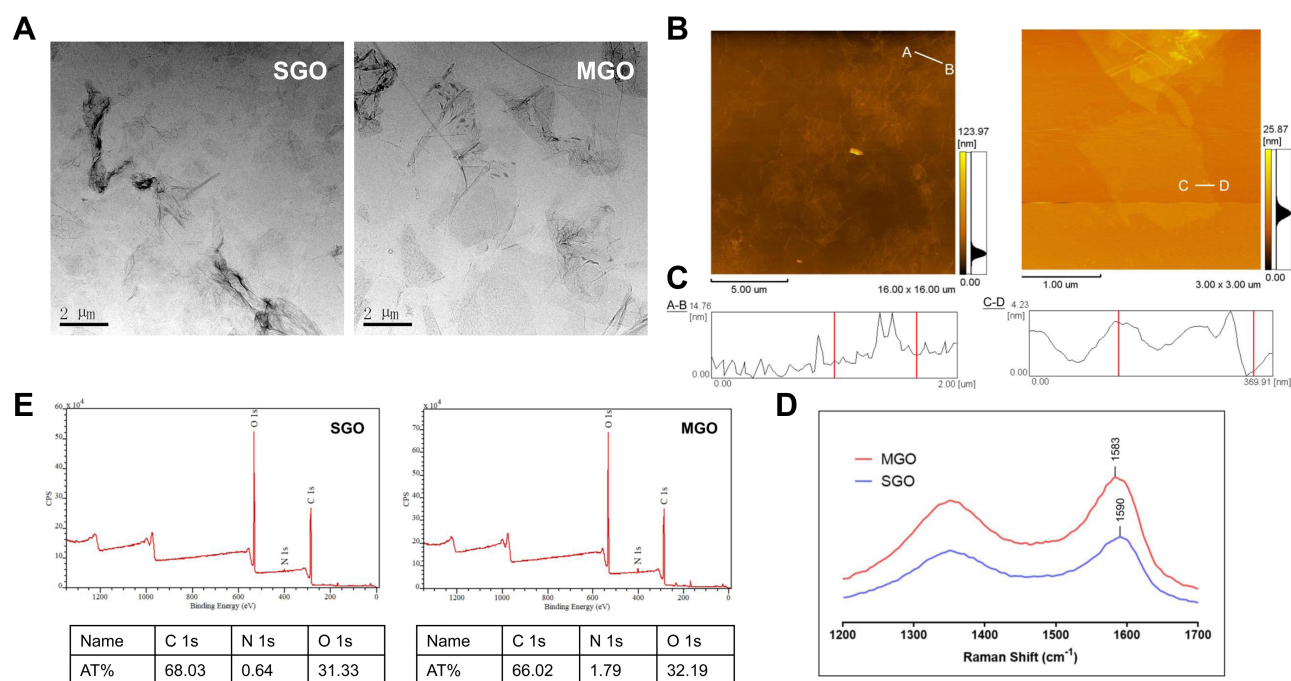


Figure 1 Characterization of graphene oxide with different sheet thickness. **(A)** Transmission electron microscope (TEM) images of SGO (left) and MGO (right). **(B and C)** Atomic force microscope (AFM) image of the morphology and the thickness of SGO (left) and MGO (right). **(D)** Raman spectra of MGO and SGO, collected at 532 nm excitation. **(E)** XPS mapping of SGO and MGO.

a lower energy, which meant that an increase in the number of layers could slightly soften the bonds.

X-ray diffraction (XRD) was also performed to investigate the structure of SGO and MGO and the results have been supplemented in [Figure S2](#). Both SGO and MGO showed diffraction peak at $2\theta \approx 11^\circ$ which corresponding to the (001) crystal plane of graphene oxide. While the diffraction peak intensity of SGO is much weaker than MGO for the interlaminar exfoliation of single-layer graphene oxide. Therefore, the XRD data are in good agreement with the expected single and multi-layer structure of graphene oxide.

Previous research has revealed that the oxidation degree of GO can affect its regulation ability on the self-renewal of ESCs.³⁵ Therefore, we analyzed the contents of C and O through XPS to verify if there was a significant difference in oxygen content between SGO and MGO ([Figure 1E](#)). The At.% contents of C1s and O1s were 68.03% and 31.33% in SGO, respectively. The contents of C1s and O1s were 66.02% and 32.19% in MGO, respectively. Thus, there was no significant difference in oxygen content between the two kinds of samples, which indicated that the difference in regulation ability in mESCs between SGO and MGO was not caused by the difference in oxygen content of GOs.

Biocompatibility Evaluation of Graphene Oxide Nanosheets

To evaluate the cytotoxicity of GO at different sheet thicknesses, we detected the cell viability of mESCs treated with SGO and MGO at different concentrations through CCK-8. We found that both SGO and MGO, at concentrations of 8–32 $\mu\text{g/mL}$, showed negligible toxicity after incubating with mESCs for 24 h or 48 h ([Figure 2A](#)). Furthermore, annexin V-FITC/PI dual staining was used to assess whether SGO or MGO would induce the apoptosis of mESCs ([Figure 2B](#)). The cells were treated with 8–32 $\mu\text{g/mL}$ of either SGO or MGO for 48 h, and no significant apoptosis or necrosis were observed in any group; The cell survival rate of all the groups treated with GOs at selected concentrations were above 80% to compared with LIF- group. To further confirm the cytotoxicity of SGO and MGO toward mESCs, we detected the ROS level in mESCs after treatment with SGO and MGO at a concentration of 16 $\mu\text{g/mL}$ ([Figure 2C](#)). The levels were not significantly different from those in a negative control group, but both were significantly lower than those in a positive control group. Thus, neither SGO nor MGO caused an oxidative stress response of mESCs at certain concentrations.

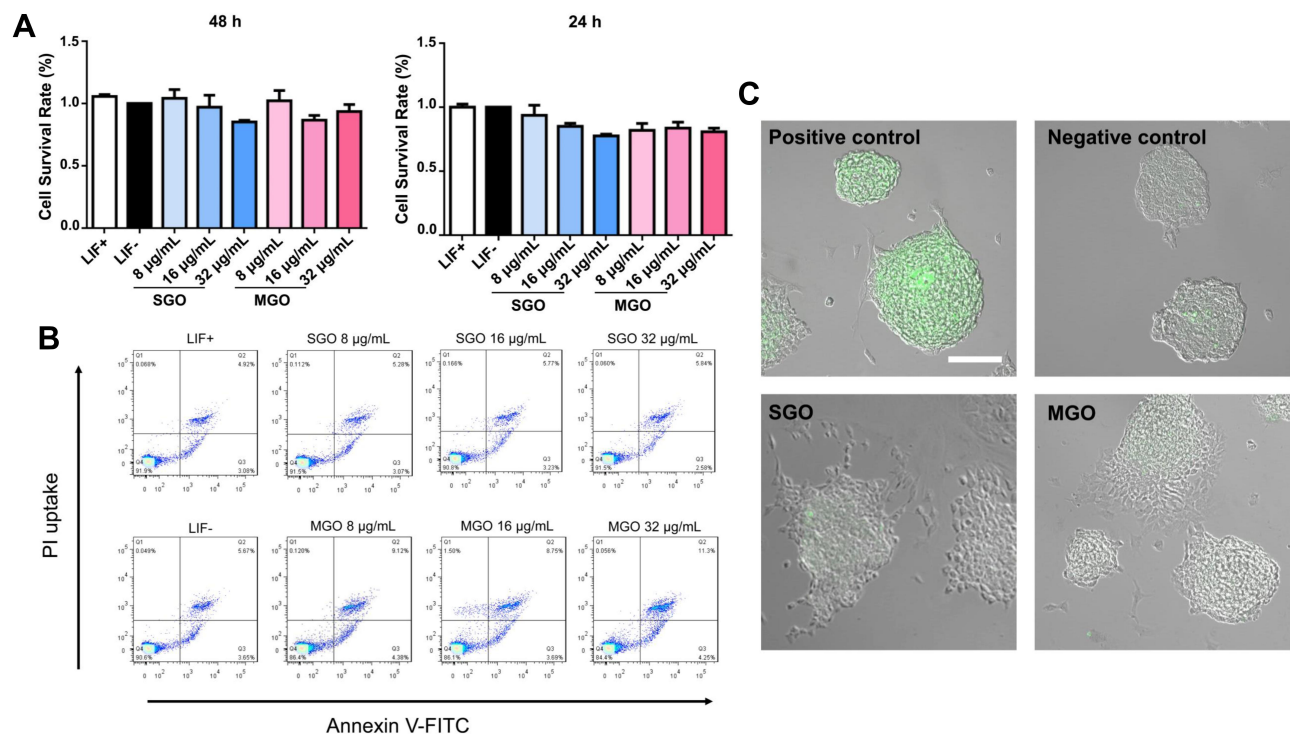


Figure 2 Influence of graphene oxide nanosheets on cell viability, apoptosis, and oxidative stress. **(A)** CCK-8 was performed to analyze the viability of mESCs after being separately treated with SGO and MGO for 24 h and 48 h. Data are expressed as the mean \pm SEM. **(B)** Annexin V-FITC/PI dual staining was used to detect the apoptosis of mESCs after incubation with SGO and MGO for 48 h. **(C)** Intracellular ROS levels of mESCs treated with SGO or MGO for 48 h. Cells in the positive control group were cultivated with the addition of Rosup. The ROS levels were labeled by oxidized fluorescent probe DCFH-DA and observed through a laser scanning confocal microscope. Scale bars: 50 μm .

These data demonstrate that both SGO and MGO are biocompatible with mESCs at concentrations \leq 32 $\mu\text{g/mL}$.

Thickness Effects of GO Nanosheets on Pluripotency of mESCs

To evaluate the effect of GOs with different sheet thickness on the self-renewal of mESCs, feeder-free mESCs were cultivated in the absence of LIF and with the addition of MGO or SGO. Feeder-free mESCs cultured with or without LIF were treated as a positive control and negative control, respectively. The cell morphology and alkaline phosphatase (ALP) expression of mESCs were observed by ALP staining in Figure 3A. The expression of ALP was significantly higher in MGO-treated mESCs than in SGO-treated cells, and the morphology of mESCs in the SGO-treated group was more differentiated. However, SGO had a slightly higher effect on the self-renewal of mESCs than did the LIF- group.

RT-PCR was used to quantify the expression of pluripotent markers *Oct4*, *Nanog*, *Sox2*, and *Esrrb* at transcriptional levels after separate treatments with SGO and MGO

for 3 days in Figure 3B. The expression of all four self-renewal markers was significantly higher in MGO-treated mESCs than in the LIF- and SGO-treated groups. However, there were no significant differences in the self-renewal markers between the SGO-treated and LIF- group. These results indicate that MGO significantly maintained the expression of pluripotent genes in mESCs, whereas SGO did not. To further verify the effect of SGO and MGO treatment on the expression of pluripotent markers, a Western blot was performed to investigate the expression of pluripotent proteins OCT4, NANOG, ESRRB, and SSEA-1 in Figure 3C. Their expressions in mESCs were higher after treatment with MGO than in the SGO and LIF- group, but there were no significant differences compared to the LIF+ group. However, the levels of pluripotent proteins expressed in SGO-treated mESCs were reduced more significantly than those in the LIF+ group, further proving that MGO effectively maintained the expression of pluripotent genes in mESCs, while SGO did not. In addition, immunofluorescence staining was performed to investigate the change in pluripotent markers OCT4 and SOX2 in mESCs after being separately treated with SGO and MGO. The images in Figure 3D and the

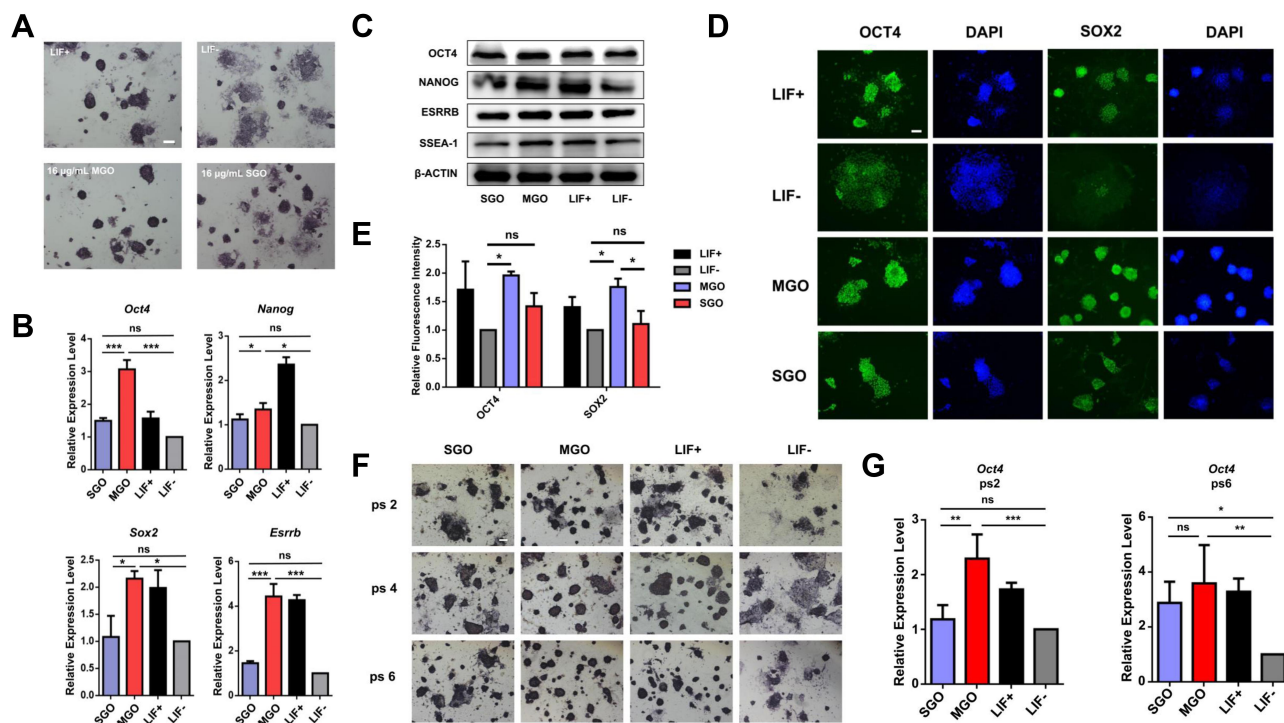


Figure 3 Effects of thickness of graphene oxide nanosheets on pluripotency of mouse embryonic stem cells. **(A)** Alkaline phosphatase (ALP) staining of feeder-free mESCs treated with two thicknesses of GOs at a concentration of 16 µg/mL for 3 days. Scale bars: 250 µm. **(B)** RT-PCR assay reflecting the relative mRNA expression of self-renewal markers *Oct4*, *Nanog*, *Sox2*, and *Esrrb* after being separately treated with 16 µg/mL SGO and 16 µg/mL MGO for 3 days. **(C)** Western blot analyses of the expression levels of OCT4, NANOG, ESRRB, and SSEA-1 in mESCs after incubation with 16 µg/mL SGO or 16 µg/mL MGO for 3 days. **(D)** Immunostaining of OCT4 and SOX2 in mESCs separately treated with 16 µg/mL of two thicknesses of GOs for 3 days. Nuclei were stained with DAPI (blue). Scale bars: 100 µm. **(E)** The relative fluorescence intensity quantification of **(D)**. **(F)** ALP staining of mESCs after treated with 16 µg/mL SGO or MGO at passages 2, 4, and 6. Scale bars: 250 µm. **(G)** The RT-PCR assay reflected the relative mRNA expression of *Oct4* after separate treatment with 16 µg/mL SGO and 16 µg/mL MGO at passages 2 and 6. All data are the mean ± SEM (n=3, ***p < 0.001, **p < 0.01, *p < 0.05, ns means there was no significant difference between the two groups).

fluorescent quantification in Figure 3E show that the relative fluorescence expression in MGO-treated mESCs was significantly higher than that in the LIF⁻ group, but there were no significant differences between the SGO-treated group and LIF⁻ group. Meanwhile, the cell morphology maintained an undifferentiated state in the MGO-treated group, while the cells showed some degree of morphodifferentiation in the SGO-treated group.

To examine the effects of MGO and SGO on the self-renewal of mESCs during the long-term culture process, the expressions of ALP and self-renewal genes from passages 2–6 were tracked. ALP staining results are shown in Figure 3F. Compared to the SGO and LIF⁻ groups, MGO effectively sustained the expression of ALP and maintained the clonal morphology in passages 2, 4, and 6. Compared to the LIF⁻ group, SGO slightly maintained the clonal morphology of mESCs to a certain degree, but the effect was less significant than that of MGO. However, the expression of ALP in SGO-treated cells was upregulated with an increase in passages, and the clonal morphology of cells was gradually clear. RT-PCR was applied for

the further detection of pluripotent gene *Oct4* at passages 2 and 6. As shown in Figure 3G, when cells were transferred to the second passage, the expression of *Oct4* in the MGO-treated group exceeded that in the SGO and LIF⁻ groups, while the expression of *Oct4* in the SGO group was not significantly upregulated compared to that in the LIF⁻ group. In passage 6, the expression of *Oct4* appeared to significantly increase compared to the LIF⁻ group; this is consistent with the ALP staining results in that, with an increase in passage in mESCs, both SGO and MGO maintain the self-renewal of mESCs but MGO is more effective than SGO.

Effects of GO Thickness on Differentiation Potential of mESCs

ESCs have the potential to differentiate into various types of cells, and their differentiation potential can be verified by both in vitro and in vivo experiments, particularly by the natural induction method in vitro. After removing feeder cells and LIF, single, dissociated ESCs may gather

under a suspension culture to form embryoid bodies (EBs) and express three germ layer genes. Teratoma is a tumor derived from primitive germ cells, and its formation can be applied to verify the differentiation potential of mESCs *in vivo*. Teratomas may form after implanting dissociated mESCs into the subcutaneous layer of nude mice. The rate of teratoma formation is determined by the differentiation potential of cells, where higher differentiation potentials lead to faster tumor formation rates.

The EBs shown in Figure 4A were formed at day 4 after mESC incubation in MGO and SGO for 3 days. Both the LIF+ group and MGO-treated mESCs formed complete and uniform EBs. However, only a few cells formed clusters in the SGO-treated and LIF- groups. Moreover, the clustered cells were nonuniform and had more cell fragments. This indicates that the cells after MGO treatment still maintained their differentiation potential, but SGO influenced this potential.

Next, SGO-treated and MGO-treated mESCs were injected into the subcutaneous layer of nude mice, forming teratomas after 4 weeks, as shown in Figure 4B (the

LIF+ group and LIF- group acted as controls). The weight and volume of the tumors were quantified (Figure 4C and D), which showed that the teratomas were significantly larger in the MGO-treated group than in the LIF- and SGO-treated groups in terms of both weight and volume, and there were no significant differences compared to the LIF+ group. Histological examination was performed to detect the typical differentiated tissues of all three germ layers (Figure 4E). The respiratory epithelium from the endoderm, myoideum, adipose tissue and cartilage tissue from the mesoderm, and horny epithelium from the ectoderm were detected in the MGO-treated group, while only respiratory epithelium from the endoderm and bone tissue and adipose tissue from the mesoderm were detected from the SGO-treated group. The formation of teratomas further indicated that mESCs treated by MGO still maintained their differentiation potential after long cultivation times. In contrast, long-term SGO-treated mESCs sustained a certain level of differentiation potential but significantly less than MGO-treated mESCs.

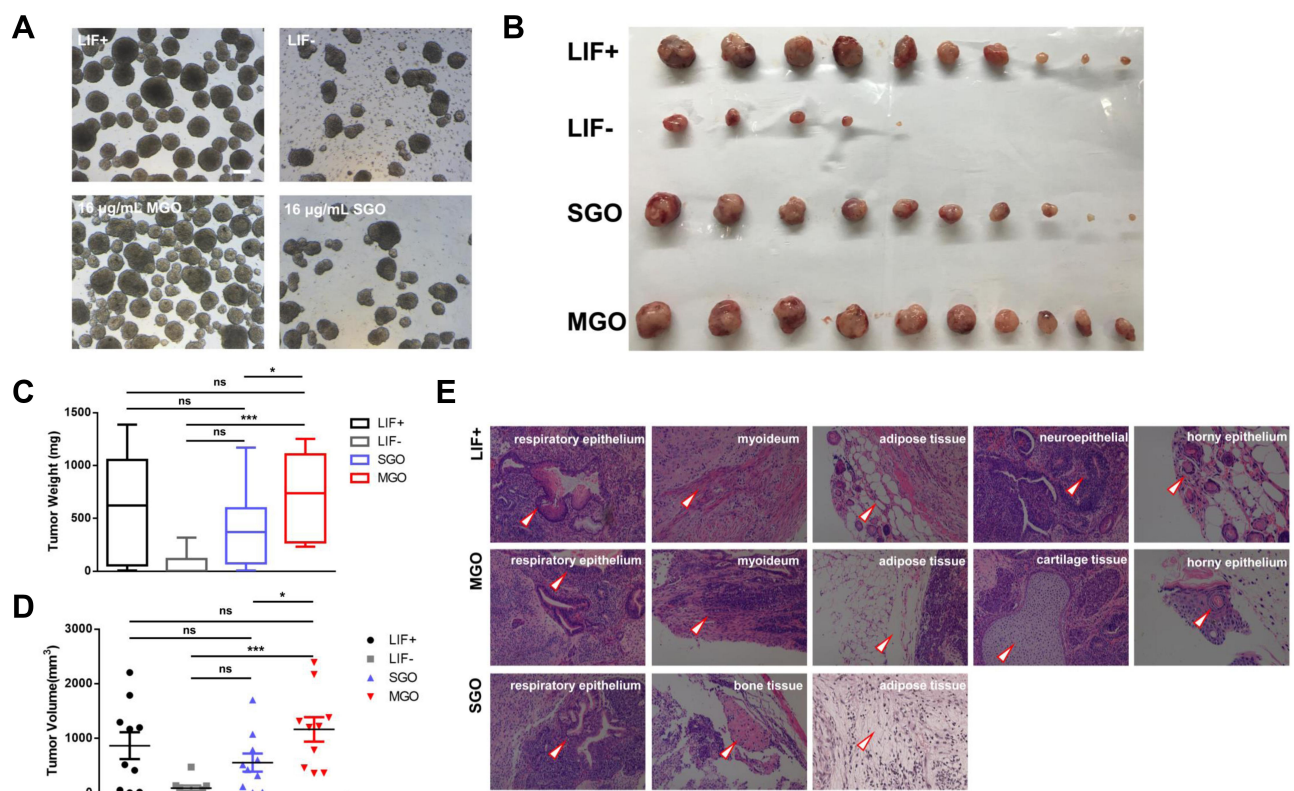


Figure 4 Effects of thickness of graphene oxide on differentiation potential of mouse embryonic stem cells. (A) EBs formed by mESCs treated with the two types of GOs at a concentration of 16 µg/mL for 3 days. Scale bars: 250 µm. (B) Comparison of teratomas formed subcutaneously in nude mice after injected SGO- or MGO-treated mESCs at passage 3, and the quantification of tumor weight (C) and volume (D). All data are the mean ± SEM (n=10, ***p < 0.001, *p < 0.05, ns means there was no significant difference between the two groups). (E) HE staining of teratomas formed in MGO- or SGO-treated mESCs. (The arrow heads indicate three embryonic germ layers of different tissues.).

Effects of Thickness of Graphene Oxide Nanosheets on the Interaction Between ECM Proteins and Integrins of Mouse Embryonic Stem Cells

In previous research, we demonstrated that GO sustained the self-renewal of mESCs by regulating the downstream pathways of the integrin signal.²³ However, it could not pass through the cytomembrane of MSCs at micro-sizes.⁴³ Even when the size of GO was as small as 400 nm, only a few were located in the cytoplasm of NSCs; such a low concentration of GO in the cytoplasm would not affect the behavior of cells.⁴⁴ The clonal morphology of mESCs were observed by SEM after the addition SGO and MGO in [Figure S3](#) to show the comparison of the mESCs binding with SGO and MGO. The control group without adding each kind of GO exhibits the obvious boundary of each cell and the cell aggregation structure. However, at SGO and MGO treatment groups, the boundary between cells were not obvious and there appeared to be material wrapped around the outside of the aggregated cells. To test whether GOs can pass through an mESC membrane, FITC-labeled SGO or MGO were incubated with mESCs for 16 h, and the distribution of SGO or MGO was observed through confocal microscopy. Almost all of the SGO and MGO was distributed at the outside of the cell membrane and nearly no fluorescence could be observed inside the cells ([Figure 5A](#)), indicating that neither type of GO can pass through the membrane of mESCs and thus that GO does not directly interact with intracellular molecules but rather regulates the self-renewal of mESCs by interacting with the extracellular environment.

Therefore, we further hypothesized that GO regulates the downstream signaling pathway of integrin by interacting with ECM components, and that GOs with different layer thicknesses possess different regulatory capacities for this process. Franqui et al demonstrated that SGO and MGO interact with FBS proteins in a DMEM medium could forming distinct protein corona composition and the different proteins enriched within SGO and MGO are involved in distinct biological processes.⁴⁵ Our previous studies have shown that the addition of FN to a culture system can inhibit the ability of GO to maintain the self-renewal of mESCs.²³ Therefore, we detected the binding capacity of both SGO and MGO with total proteins in FBS and BSA as well as with FN. The concentration of adsorbed protein was also quantified in [Figure 5B](#), which

indicated that there were no significant differences in the binding capacity of SGO and MGO with FBS and BSA, while that of MGO with FN was significantly higher than that of SGO. The binding ability between SGO/MGO and FN was also detected by TEM. The results in [Figure S4](#) display a higher electronic density distribution on the surface of MGO than SGO and MGO shows more obvious folding and accumulation than SGO, which might be attributed to the tight binding ability between FN and MGO.

The difference binding ability of FN with SGO and MGO may be caused by the surface mechanical properties of GO sheets with different thicknesses. The adsorption capacity of carbon material to protein is related to the surface curvature of carbon material, and increases with a decrease in curvature.^{46,47} Compared to MGO, the morphology of SGO would present twists and change from 2D to 3D spontaneously to reduce its own surface energy. Therefore, the folds formed on SGO were significantly larger than those on MGO, resulting in a difference in FN adsorption capacity. This suggests that the binding capacity of different GOs with FN in ECM could be a key factor regulating the self-renewal of mESCs.

Integrin $\alpha 5 \beta 1$ is a specific receptor of FN, which can be found in various adhesion structures and regulates the proliferation and differentiation of cells.⁴⁸ A Western blot was performed to investigate if the specific adsorption of GOs with FN may influence the expression of integrin $\alpha 5 \beta 1$. The expressions of integrin $\alpha 5$ and integrin $\beta 1$ in mESCs were detected after being separately treated with SGO and MGO, and the results ([Figure 5C](#) and [D](#)) indicated that MGO more significantly downregulated the expression of integrin $\alpha 5$ and integrin $\beta 1$ than did SGO. In addition, the expression level of integrins could influence its downstream proteins, such as p-FAK, Vinculin, p-ERK1/2, and RAP1. Therefore, we investigated the expression of these proteins after treatment with SGO and MGO. The results ([Figure 5E](#)) revealed that their expressions were significantly higher in the SGO group than in the MGO group. This further illuminates the fact that SGO and MGO possess different capacities for regulating the downstream proteins of integrins, and that MGO has a stronger inhibitory capacity than SGO. Immunofluorescence was also used to observe the expressions of integrin $\alpha 5$, integrin $\beta 1$, and OCT4 in mESCs after 3 days treatments with SGO and MGO. The fluorescence intensity of integrin $\alpha 5$ and integrin $\beta 1$ was significantly lower in the MGO group than in the SGO and LIF-

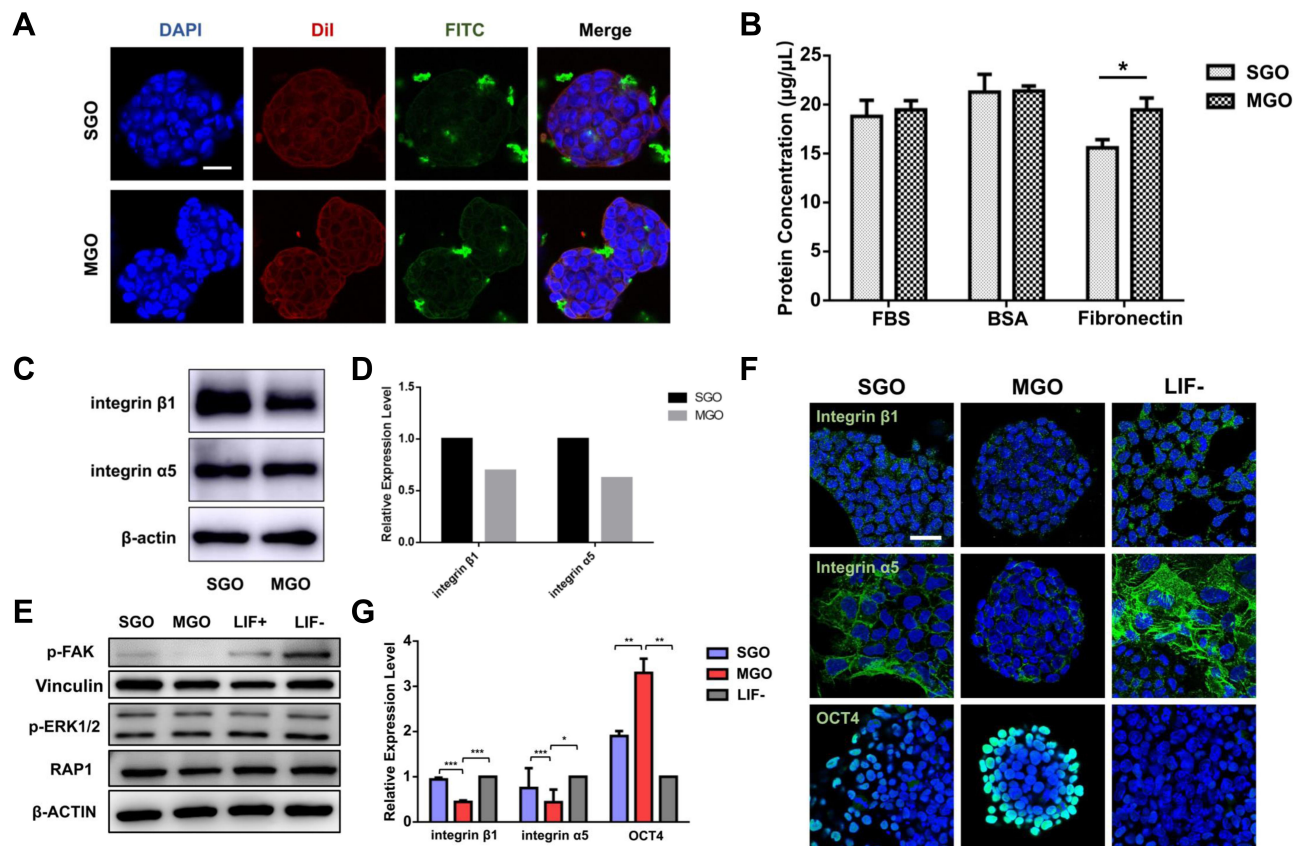


Figure 5 Effects of thickness of graphene oxide nanosheets on the interaction between ECM proteins and integrins in mouse embryonic stem cells. **(A)** Confocal laser scanning micrographs indicate the localization of FITC-conjugated SGO and MGO in mESCs. The cytomembrane was labeled with DiI (red) and nuclei were stained with DAPI (blue). Scale bars: 25 µm. **(B)** The adsorption capacity of FBS, BSA, and FN with SGO or MGO. (n=3, *p < 0.05). **(C and D)** Western blot analysis and densitometric quantification of integrin α5 and integrin β1 expression levels in mESCs cultured with the addition of 16 µg/mL SGO and MGO in medium for 3 days. **(E)** Pivotal genes downstream of the integrin signaling pathway were verified by Western blot after separate treatment with 16 µg/mL SGO and MGO for 3 days. **(F and G)** Immunostaining and fluorescence intensity quantification indicated the expression of integrin α5, integrin β1, and OCT4 (green) in mESCs treated with 16 µg/mL SGO or MGO for 3 days. Nuclei were stained with DAPI (blue). Scale bars: 25 µm. ***p < 0.001, **p < 0.01 *p < 0.05).

groups, while that of OCT4 was significantly increased (Figure 5F and G).

These results prove that the specific adsorption of layered GOs of different thickness on FN affects the interaction between FN and its receptor integrin α5β1, thus regulating the intracellular signaling pathways of mESCs.

We found that MGO inhibits the expression of integrin α5 and integrin β1 by interacting with FN, thus upregulating the expression of self-renewal markers through the intracellular signaling pathway and maintaining the self-renewal of mESCs. To verify this conclusion, anti-integrin α5 and anti-integrin β1 were used to block the surface receptor integrin α5β1 on mESCs and thus depress the activation of its downstream signal pathways. The cell morphologies of mESCs with integrin α5, integrin β1, and integrin α5β1 blocked for 3 days are shown in Figure 6A; these cell clones exhibited clear boundaries

and displayed the typical colony morphology compared to the LIF- group. The expression of self-renewal markers and downstream proteins of integrins were detected via Western blot after treatment with anti-integrin α5, anti-integrin β1, and anti-integrin α5+anti-integrin β1 (anti-integrin α5+β1) in Figure 6B. The expressions of p-FAK, Vinculin, p-ERK1/2, and RAP1 were significantly restrained after being blocked by anti-integrin α5 and anti-integrin β1 compared to the LIF- group, and the inhibition was more pronounced in the anti-integrin α5+β1 group. These results indicate that anti-integrin α5 and anti-integrin β1 effectively blocked integrin α5 and integrin β1, thus inhibiting the expression of their downstream genes. The expressions of pluripotent genes of the mESCs after blocking for 3 days showed that the expression tendency of OCT4, NANOG, and SOX2 were opposite to that of the integrin downstream genes. Compared to the LIF- group, the expressions of OCT4, NANOG, and

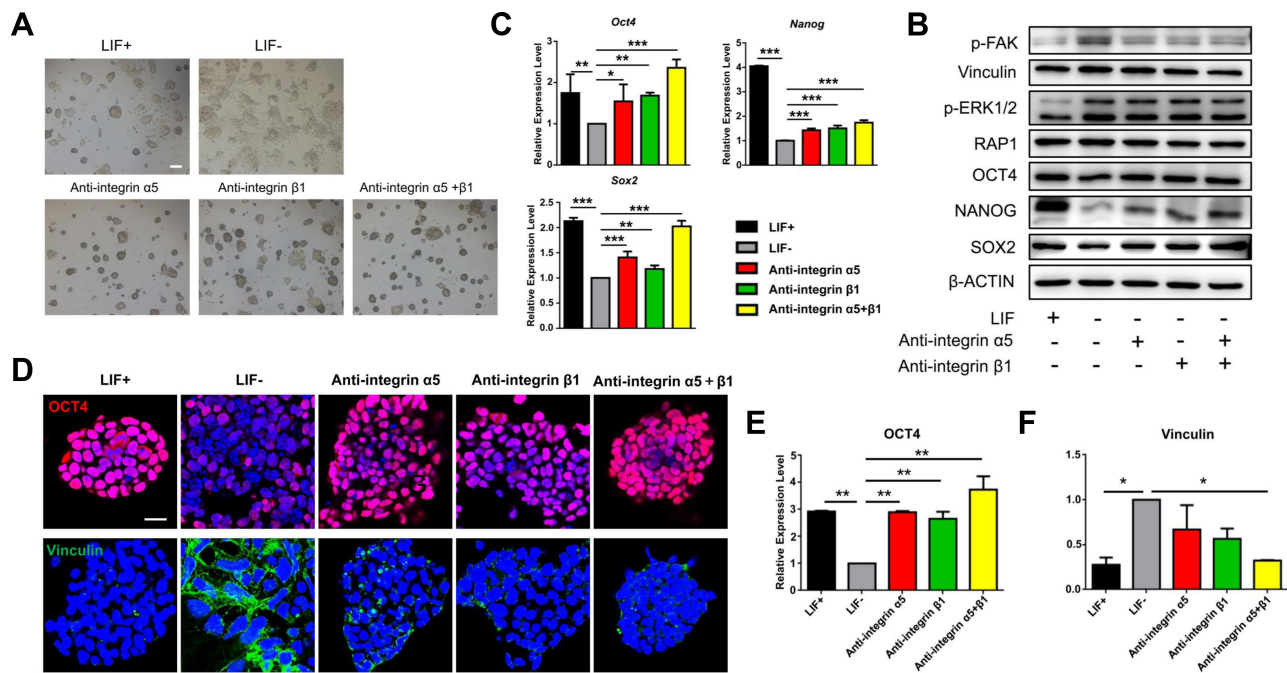


Figure 6 Effects of inhibiting the interaction between ECM proteins and integrins on the self-renewal of mESCs. **(A)** Cell morphology of mESCs after being blocked with anti-integrin $\alpha 5$, anti-integrin $\beta 1$, and anti-integrin $\alpha 5$ +anti-integrin $\beta 1$ (anti-integrin $\alpha 5$ + $\beta 1$) for 3 days. Scale bars: 250 μ m. **(B)** The proteins downstream of the integrin signaling pathway (p-FAK, Vinculin, p-ERK1/2, and RAP1) and pluripotent proteins (OCT4, NANOG, and SOX2) were verified by Western blot after separately treating them with each compound. **(C)** RT-PCR detected the self-renewal markers *Oct4*, *Nanog*, and *Sox2* in mESCs blocked for 3 days. **(D)** The expressions of OCT4 (red) and Vinculin (green) in mESCs treated with each compound for 3 days were evaluated via immunostaining and fluorescence intensity quantification (**E** and **F**). Nuclei were stained with DAPI (blue). Scale bars: 25 μ m. All data are the mean \pm SEM ($n=3$, *** $p < 0.001$, ** $p < 0.01$, * $p < 0.05$).

SOX2 in groups treated with anti-integrin $\alpha 5$ and anti-integrin $\beta 1$ were upregulated. In addition, these genes presented a more significant upregulation in the group treated with anti-integrin $\alpha 5$ + $\beta 1$. Further quantitative analyses were conducted by RT-PCR on the expression of the pluripotent genes *Oct4*, *Nanog*, and *Sox2* at the transcription level in mESCs after blocking by anti-integrin $\alpha 5$, anti-integrin $\beta 1$, and anti-integrin $\alpha 5$ + $\beta 1$ for 3 days. These expressions were significantly increased after blocking with anti-integrin $\alpha 5$ and anti-integrin $\beta 1$ compared to the LIF- group, and all three pluripotent genes simultaneously exhibited extremely significant expression increases in the anti-integrin $\alpha 5$ + $\beta 1$ group (Figure 6C). This trend was also consistent with the expression levels of pluripotent proteins (Figure 6B). These results all demonstrate that the inactivation of integrin $\alpha 5\beta 1$ promotes the self-renewal of mESCs.

Integrins may affect cell adhesion by regulating the expression of their downstream proteins. Vinculin is a downstream protein of integrin and a crucial component of focal adhesion, whose formation may regulate the adhesion ability of cells to the ECM.⁴⁹ The results in Figure 6D–F exhibited that the expression of Vinculin receded in

both the group treated with anti-integrin $\alpha 5$ and that treated with anti-integrin $\beta 1$, and the expression of Vinculin in the group treated with anti-integrin $\alpha 5$ + $\beta 1$ was reduced to an even greater extent. However, the expression trend of OCT4 was contrary to that of Vinculin. These results further demonstrate that the self-renewal ability of mESCs decreases with an increase in cell adhesion.

Conclusion

This study, based on a previous discovery that GO sustains the self-renewal of mESCs, compared the effects of SGO and MGO in regulating pluripotency. In summary, both SGO and MGO had good biocompatibility with mESCs at a concentration under 32 μ g/mL. However, only MGO possessed effective biofunction in sustaining the self-renewal ability and differentiation potential of mESCs. SGO hardly sustained the self-renewal of mESCs and also influenced the differentiation potential of mESCs. Neither SGO nor MGO passed through the cytomembrane of mESCs. The adsorption ability of MGO to FN was stronger than that of SGO. This specific adsorption influenced the interaction between the ECM protein FN and its receptor integrin $\alpha 5\beta 1$ and thus regulated the pluripotency

of mESCs, potentially demonstrating a pivotal extracellular mechanism of GO in maintaining the self-renewal of mESCs. We assume that the adsorption difference may be caused by the fold or twist differences between SGO and MGO. In conclusion, this research lays the theoretical foundation for the application of GO to regulate the cell fate of mESCs and provides a new concept for designing innovative functional nanomaterials for the regulation of the behavior of stem cells.

Acknowledgments

This work was financially supported by the National Key Research and Development Program (Grant No. 2016YFA0100800), the National Natural Science Foundation of China (Grant No. 31770923, 31727801, 32071401) and the Shanghai Natural Science Foundation (Grant No. 20ZR1461600).

Disclosure

Dr Guoxin Jing reports grants from the National Key Research and Development Program, the National Natural Science Foundation of China, and the Shanghai Natural Science Foundation, during the conduct of the study. There are no other conflicts to declare.

References

- Smith AG. Embryo-derived stem cells: of mice and men. *Annu Rev Cell Dev Biol.* 2001;17:435–462. doi:10.1146/annurev.cellbio.17.1.435
- Doğan A. Embryonic stem cells in development and regenerative medicine. *Adv Exp Med Biol.* 2018;1079:1–15.
- Yamanaka S. Pluripotent stem cell-based cell therapy—Promise and challenges. *Cell Stem Cell.* 2020;27(4):523–531. doi:10.1016/j.stem.2020.09.014
- Young RA. Control of the embryonic stem cell state. *Cell.* 2011;144(6):940–954. doi:10.1016/j.cell.2011.01.032
- Deb KD, Griffith M, De Muinck E, Rafat M. Nanotechnology in stem cells research: advances and applications. *Front Biosci.* 2012;17(1):1747–1760. doi:10.2741/4016
- Dong Y, Wu X, Chen X, et al. Nanotechnology shaping stem cell therapy: recent advances, application, challenges, and future outlook. *Biomed Pharmacother.* 2021;137:111236. doi:10.1016/j.biopha.2021.111236
- Wu Y, Zhu R, Zhou Y, et al. Layered double hydroxide nanoparticles promote self-renewal of mouse embryonic stem cells through the PI3K signaling pathway. *Nanoscale.* 2015;7(25):11102–11114. doi:10.1039/C5NR02339D
- Zhu R, Zhu X, Zhu Y, et al. Immunomodulatory layered double hydroxide nanoparticles enable neurogenesis by targeting transforming growth factor- β receptor 2. *ACS Nano.* 2021;15(2):2812–2830. doi:10.1021/acsnano.0c08727
- Wang G, Zhang H, Zhao Y, et al. Noggin and BFGF cooperate to maintain the pluripotency of human embryonic stem cells in the absence of feeder layers. *Biochem Biophys Res Commun.* 2005;330(3):934–942. doi:10.1016/j.bbrc.2005.03.058

- Williams RL, Hilton DJ, Pease S, et al. Myeloid leukaemia inhibitory factor maintains the developmental potential of embryonic stem cells. *Nature.* 1988;336(6200):684–687. doi:10.1038/336684a0
- Dickinson LE, Kusuma S, Gerecht S. Reconstructing the differentiation niche of embryonic stem cells using biomaterials. *Macromol Biosci.* 2011;11(1):36–49. doi:10.1002/mabi.201000245
- Xu C, Inokuma MS, Denham J, et al. Feeder-free growth of undifferentiated human embryonic stem cells. *Nat Biotechnol.* 2001;19(10):971–974. doi:10.1038/nbt1001-971
- Ying QL, Wray J, Nichols J, et al. The ground state of embryonic stem cell self-renewal. *Nature.* 2008;453(7194):519–523. doi:10.1038/nature06968
- Sasse J, Hemmann U, Schwartz C, et al. Mutational analysis of acute-phase response factor/stat3 activation and dimerization. *Mol Cell Biol.* 1997;17(8):4677–4686. doi:10.1128/MCB.17.8.4677
- Ramirez F, Rifkin DB. Cell signaling events: a view from the matrix. *Matrix Biol.* 2003;22(2):101–107. doi:10.1016/S0945-053X(03)00002-7
- Wang H, Luo X, Leighton J. Extracellular matrix and integrins in embryonic stem cell differentiation. *Biochem Insights.* 2015;8(Suppl 2):15–21. doi:10.4137/BCI.S30377
- Hynes RO. Integrins: bidirectional, allosteric signaling machines. *Cell.* 2002;110(6):673–687. doi:10.1016/S0092-8674(02)00971-6
- Barczyk M, Carracedo S, Gullberg D. Integrins. *Cell Tissue Res.* 2010;339(1):269–280. doi:10.1007/s00441-009-0834-6
- Darribère T, Skalski M, Cousin H, et al. Integrins: regulators of embryogenesis. *Biol Cell.* 2000;92(1):5–25. doi:10.1016/S0248-4900(00)88760-2
- Fuchs E, Tumber T, Guasch G. Socializing with the neighbors: stem cells and their niche. *Cell.* 2004;116(6):769–778. doi:10.1016/S0092-8674(04)00255-7
- Pankov R, Yamada KM. Fibronectin at a Glance. *J Cell Sci.* 2002;115(20):3861–3863. doi:10.1242/jcs.00059
- Larsen M, Artym VV, Green JA, et al. The matrix reorganized: extracellular matrix remodeling and integrin signaling. *Curr Opin Cell Biol.* 2006;18:463–471. doi:10.1016/j.ccb.2006.08.009
- Jing G, Wang Z, Zhuang X, et al. Suspended graphene oxide nanosheets maintain the self-renewal of mouse embryonic stem cells via down-regulating the expression of vinculin. *Biomaterials.* 2018;171:1–11. doi:10.1016/j.biomaterials.2018.04.017
- Li X, Wang X, Zhang L, et al. Chemically derived, ultrasmooth graphene nanoribbon semiconductors. *Science.* 2008;319(5867):1229–1232. doi:10.1126/science.1150878
- Stankovich S, Dikin DA, Dommett GHB, et al. Graphene-based composite materials. *Nature.* 2006;442(7100):282–286. doi:10.1038/nature04969
- Seabra AB, Paula AJ, De Lima R, et al. Nanotoxicity of graphene and graphene oxide. *Chem Res Toxicol.* 2014;27(2):159–168. doi:10.1021/tx400385x
- Georgakilas V, Tiwari JN, Kemp KC, et al. Noncovalent functionalization of graphene and graphene oxide for energy materials, biosensing, catalytic, and biomedical applications. *Chem Rev.* 2016;116(9):5464–5519. doi:10.1021/acs.chemrev.5b00620
- Guo W, Wang S, Yu X, et al. Construction of a 3D rGO-collagen hybrid scaffold for enhancement of the neural differentiation of mesenchymal stem cells. *Nanoscale.* 2016;8(4):1897–1904. doi:10.1039/C5NR06602F
- Choe G, Oh S, Seok JM, et al. Graphene oxide/alginate composites as novel bioinks for three-dimensional mesenchymal stem cell printing and bone regeneration applications. *Nanoscale.* 2019;11(48):23275–23285. doi:10.1039/C9NR07643C
- Halim A, Luo Q, Ju Y, et al. A mini review focused on the recent applications of graphene oxide in stem cell growth and differentiation. *Nanomaterials.* 2018;8:736(16):1517–1521. doi:10.1016/0006-2952(75)90029-5

31. Wei C, Liu Z, Jiang F, et al. Cellular behaviours of bone marrow-derived mesenchymal stem cells towards pristine graphene oxide nanosheets. *Cell Prolif.* 2017;50(5):e12367. doi:10.1111/cpr.12367
32. Akhavan O, Ghaderi E, Akhavan A, et al. Size-dependent genotoxicity of graphene nanoplatelets in human stem cells. *Biomaterials.* 2012;33(32):8017–8025. doi:10.1016/j.biomaterials.2012.07.040
33. Lin L, Zhuang X, Huang R, et al. Size-dependent effects of suspended graphene oxide nanoparticles on the cellular fate of mouse neural stem cells. *Int J Nanomedicine.* 2020;15:1421–1435. doi:10.2147/IJN.S225722
34. Talukdar Y, Rashkow JT, Lalwani G, et al. The effects of graphene nanostructures on mesenchymal stem cells. *Biomaterials.* 2014;35(18):4863–4877. doi:10.1016/j.biomaterials.2014.02.054
35. Zhao J, Tang M, Cao J, et al. Structurally tunable reduced graphene oxide substrate maintains mouse embryonic stem cell pluripotency. *Adv Sci.* 2019;6(12):1802136. doi:10.1002/advs.201802136
36. Kumar S, Parekh SH. Molecular control of interfacial fibronectin structure on graphene oxide steers cell fate. *ACS Appl Mater Interfaces.* 2021;13(2):2346–2359. doi:10.1021/acsami.0c21042
37. Lee JH, Shin YC, Jin OS, et al. Reduced graphene oxide-coated hydroxyapatite composites stimulate spontaneous osteogenic differentiation of human mesenchymal stem cells. *Nanoscale.* 2015;7(27):11642–11651. doi:10.1039/C5NR01580D
38. Guo W, Zhang X, Yu X, et al. Self-powered electrical stimulation for enhancing neural differentiation of mesenchymal stem cells on graphene-Poly(3,4-Ethylenedioxythiophene) hybrid microfibers. *ACS Nano.* 2016;10(5):5086–5095. doi:10.1021/acsnano.6b00200
39. Lee C, Wei X, Kysar JW, et al. Measurement of the elastic properties and intrinsic strength of monolayer graphene. *Science.* 2008;321(5887):385–388. doi:10.1126/science.1157996
40. Poot M, Van Der Zant HSJ. Nanomechanical properties of few-layer graphene membranes. *Appl Phys Lett.* 2008;92(6):063111. doi:10.1063/1.2857472
41. Wall M. The raman spectroscopy of graphene and the determination of layer thickness. *Thermo Sci.* 2011;5.
42. Wang H, Wang Y, Cao X, et al. Vibrational properties of graphene and graphene layers. *J Raman Spectrosc.* 2009;40(12):1791–1796. doi:10.1002/jrs.2321
43. Park J, Kim B, Han J, et al. Graphene oxide flakes as a cellular adhesive: prevention of reactive oxygen species mediated death of implanted cells for cardiac repair. *ACS Nano.* 2015;9(5):4987–4999. doi:10.1021/nn507149w
44. Kim J, Yang K, Lee JS, et al. Enhanced self-renewal and accelerated differentiation of human fetal neural stem cells using graphene oxide nanoparticles. *Macromol Biosci.* 2017;17(8):1–10. doi:10.1002/mabi.201600540
45. Franqui LS, De Farias MA, Portugal RV, et al. Interaction of graphene oxide with cell culture medium: evaluating the fetal bovine serum protein corona formation towards in vitro nanotoxicity assessment and nanobiointeractions. *Mater Sci Eng C Mater Biol Appl.* 2019;100:363–377. doi:10.1016/j.msec.2019.02.066
46. Raffaini G, Ganazzoli F. Surface topography effects in protein adsorption on nanostructured carbon allotropes. *Langmuir.* 2013;29(15):4883–4893. doi:10.1021/la3050779
47. Jana AK, Tiwari MK, Vanka K, et al. Unraveling origins of the heterogeneous curvature dependence of polypeptide interactions with carbon nanostructures. *Phys Chem Chem Phys.* 2016;18(8):5910–5924. doi:10.1039/C5CP04675K
48. Hunt GC, Singh P, Schwarzbauer JE, et al. Endogenous production of fibronectin is required for self-renewal of cultured mouse embryonic stem cells. *Exp Cell Res.* 2012;318(15):1820–1831. doi:10.1016/j.yexcr.2012.06.009
49. Bays JL, Demali KA. Vinculin in cell – cell and Cell – matrix adhesions. *Cell Mol Life Sci.* 2017;74(16):2999–3009. doi:10.1007/s00018-017-2511-3

International Journal of Nanomedicine

Dovepress

Publish your work in this journal

The International Journal of Nanomedicine is an international, peer-reviewed journal focusing on the application of nanotechnology in diagnostics, therapeutics, and drug delivery systems throughout the biomedical field. This journal is indexed on PubMed Central, MedLine, CAS, SciSearch®, Current Contents®/Clinical Medicine,

Journal Citation Reports/Science Edition, EMBase, Scopus and the Elsevier Bibliographic databases. The manuscript management system is completely online and includes a very quick and fair peer-review system, which is all easy to use. Visit <http://www.dovepress.com/testimonials.php> to read real quotes from published authors.

Submit your manuscript here: <https://www.dovepress.com/international-journal-of-nanomedicine-journal>